Journal of Catalysis **183,** 336–343 (1999)
Article ID jcat.1999.2402, available online at http://www.idealibrary.com on IDEAL®

Deactivation and Coke Accumulation during CO_2/CH_4 Reforming over Pt Catalysts

J. H. Bitter, K. Seshan, and J. A. Lercher[1]

Faculty of Chemical Technology, Catalytic Processes and Materials, University of Twente, P.O. Box 217, 7500 AE, Enschede, The Netherlands

Received September 23, 1998; revised December 15, 1998; accepted December 16, 1998

The deactivation of Pt catalysts used in the generation of synthesis gas via CO_2/CH_4 reforming depends strongly on the support and the metal particle size. Methods of physicochemical characterization such as X-ray absorption spectroscopy and hydrogen chemisorption suggest that carbon formation (most likely from methane) rather than sintering is the main cause of catalyst deactivation. The rate of carbon formation decreased in the order $Pt/\gamma\text{-}Al_2O_3 \gg Pt/TiO_2 > Pt/ZrO_2$. Carbon was formed on the support and on Pt. Using the stability of that carbon toward oxidation it was estimated for $Pt/\gamma\text{-}Al_2O_3$ that 90% of the carbon was located on the oxidic support. However, even for this catalyst the amount of carbon formed is sufficient to cover only 30% of the total specific surface area of the catalyst. Although carbon can be formed on the metal and the support, evidence is presented that deactivation is caused by carbon formed on the metal and is associated with overgrowth of the catalytically active perimeter between the support and the metal. The reason for the deactivation is the imbalance between the carbon-forming methane dissociation and the oxidation by chemisorbed CO_2. Active carbidic carbon seems to be transformed to a less reactive form. Catalysts having larger Pt particles (>1 nm) tend to deactivate more quickly than catalysts with smaller Pt particles.

Key Words: **coke formation; CO_2/CH_4 reforming; deactivation; Pt catalysts.**

INTRODUCTION

Deactivation by coking is a critical criterion in the design of catalysts for CO_2/CH_4 reforming. We showed earlier that Pt-based catalysts can overcome this problem (1–4). For clarity, it is important to note that for Pt/ZrO_2 earlier work from our group (1, 2) and work from others on Ni/TiO_2 (5) and Ni/La_2O_3 (6) revealed that the reforming reaction proceeds on the metal–support perimeter. For Pt/ZrO_2 we showed that CH_4 is decomposed on the metal to a reactive carbon species and H_2 (1, 2). CO_2 forms a carbonate on the support. On the perimeter the carbonate is reduced to a formate and CO by the carbon species originating from CH_4. Under reaction conditions the formate decomposes rapidly to CO and a surface hydroxyl group. Hydroxyl groups recombine and form H_2O or react further with CH_4 to CO and H_2 (steam reforming). Thus, the activity of Pt catalysts for CO_2/CH_4 reforming is markedly influenced by the support. A mechanistic explanation of the influence of the support on the stability of reforming catalyst was reported by Zhang *et al.* (6), who showed that the remarkable stability of Ni/La_2O_3 could be affiliated with enhanced CO_2 activation on the support in the form of $La_2O_2CO_3$. In this contribution we show that also the stability of Pt catalysts is strongly influenced by the support or, more precisely, by the balance between the individual reaction steps.

In general, the deactivation of CO_2 reforming catalysts is explained by two independent processes, i.e., covering of the active sites by carbonaceous deposits (6–14) or sintering of the metal particles (10, 13). The activity of catalysts that deactivated due to carbon formation could be restored by oxidative treatment (6–13). Although all of these authors agree that carbon formation is the primary reason for the catalyst deactivation, disagreement exists on the source of the carbon. In principle, all three carbon-containing species present during reforming (CH_4, CO, and CO_2) can contribute to carbon deposition. Rostrup-Nielsen and Bak Hansen showed for Ni, Ru, Rh, Pd, Ir, and Pt supported on MgO that carbon originates mainly from methane (8). This was recently confirmed by Stagg *et al.* for Pt/SiO_2 and Pt/ZrO_2 catalysts (9). Richardson and Paripatyadar claim for $Rh/\gamma\text{-}Al_2O_3$ that under CO_2 reforming conditions carbon originates mainly from CO (10), whereas Tsipouriari *et al.* claim that carbon is formed from carbon dioxide (11). The latter is in contrast with many authors (7, 12, 13, 15, 16) who showed that an excess of CO_2 in the feed stream suppresses carbon formation. This principle is also the basis of the CALCOR process (15, 16), which uses dry CO_2 reforming in an excess of CO_2 to produce pure CO. Van Keulen *et al.* showed that over Pt/ZrO_2, carbon was not formed via a secondary reaction of the CO formed, despite the fact that the Boudouart reaction ($2CO \rightleftharpoons CO_2 + C$) was feasible under the reaction conditions (17).

[1] To whom correspondence should be addressed. Fax: +31–53–4894683. E-mail: J.A.Lercher@utct.ct.utwente.nl.

0021-9517/99 $30.00

Deactivation due to sintering of the metal particles during CO_2 reforming seems less pronounced. However, some authors observed an increase in metal particle size during reforming [see Tsipouriari *et al.* for $Rh/\gamma\text{-}Al_2O_3$ (11) and Swaan *et al.* for Ni/SiO_2 (14)]. Tsipouriari *et al.* observed a fast carbon buildup on the catalyst during the first 10 min on stream (11). After this period the amount of carbon on the catalyst remained constant, while the particle size of the Rh catalyst further increased and the deactivation progressed. Consequently, deactivation of the $Rh/\gamma\text{-}Al_2O_3$ catalyst was explained by the loss of active metal surface atoms through sintering. Swaan *et al.* also observed an increase in Ni particle size during reaction (14). The contribution of sintering to deactivation was, however, seen to be minimal.

Thus, it appears that supported metal catalysts used for CO_2/CH_4 reforming suffer mainly from deactivation caused by carbon deposition on the active sites, but sintering of metal particles may also play some role. The present contribution addresses the qualitative and quantitative aspects of carbon deposition and removal during CO_2/CH_4 reforming at atmospheric pressure by means of steady-state and transient kinetic measurements, hydrogen chemisorption, and X-ray absorption spectroscopy.

METHODS

Preparation of Impregnated Catalysts

Oxide-supported Pt catalysts were prepared by the wet impregnation technique. For this purpose a solution of $H_2PtCl_6 \cdot 6H_2O$ in water (0.01 g Pt/ml) was used. The supports, which were in powder form (ZrO_2, RC-100, Gimex; TiO_2, P25, Degussa) were isostatically pressed into pellets at 4000 bar for 5 min. The pellets were crushed and sieved to obtain grains with diameters between 0.3 and 0.6 mm. $\gamma\text{-}Al_2O_3$ (AKZO, 000-3AQ) was obtained as extrudates; these were subsequently crushed and sieved to yield grains 0.3–0.6 mm in diameter. The grains were first calcined for 15 h at 1125 K (heating rate, 3 K/min) in flowing air (30 ml/min) and subsequently impregnated with the H_2PtCl_6 solution to yield a catalyst with the desired Pt loading (0.5 wt% for the catalytic measurements and 1 wt% for the EXAFS experiments). The catalyst was dried at 365 K for 2 h in a rotating evaporator followed by drying overnight at 395 K in static air. The impregnated grains were calcined at the desired temperature for 15 h (heating rate, 3 K/min). The Pt content of the catalyst was determined by atomic absorption spectroscopy.

Catalyst Testing

Typically 300 mg of catalyst was loaded into a tubular quartz reactor (inner diameter, 5 mm) which was placed in an oven. The catalyst grains were kept in place by quartz-wool plugs. A thermocouple in a quartz sleeve was placed on top of the catalyst bed to measure the catalyst temperature. The oven temperature was controlled with an Eurotherm temperature controller. The catalysts were reduced *in situ* with 5% H_2 in N_2 for 1 h at 1125 K. After reduction, the temperature was lowered in Ar to the (initial) reaction temperature and the feed gas mixture [25% CH_4 (v/v), 25% CO_2, 5% N_2, and 45% Ar with a total flow of 170 ml min^{-1}] was switched to the reactor. The reaction products were analyzed in a gas chromatograph (Varian 3300) equipped with two 3-m Carbosieve columns and a TCD.

Carbon Determination

The amount of carbon on the used catalysts was determined by oxidizing the carbon to CO_2 and CO with O_2. These pulse experiments were performed in an Altamira AMI-2000 apparatus. The used catalysts (usually 150 mg) were heated to 1125 K in a flow of 30 ml min^{-1} He to remove adsorbed water and CO_2 (other products with $m/e < 100$ were not observed). Subsequently, oxygen (pulse size 2.1×10^{-5} mol) was pulsed into the carrier gas stream (30 ml min^{-1}). The reaction products [CO ($m/e = 28$) and CO_2 ($m/e = 44$)] were quantified with a mass spectrometer.

To estimate the fraction of the total BET surface area of the catalyst covered by carbon, it was assumed to have the same density as in benzene. The area of the benzene molecule was assumed to be 0.36 nm^2. No specific ordering or packing on the surface was assumed.

EXAFS Measurements

EXAFS measurements were performed at the Synchrotron Facility in Daresbury (beamline 9.2). The catalyst powder was pressed into a self-supporting wafer (110 mg). The catalysts were reduced *ex situ* at the desired temperature. Prior to the EXAFS experiments catalysts were rereduced *in situ* at 775 K. EXAFS measurements were carried out at liquid nitrogen temperature. To isolate the EXAFS from the X-ray absorption edge, a polynomial function characteristic of the background was subtracted. The oscillations were normalized by the mass area loading of Pt. The oscillations were k^2 weighted and Fourier transformed within the limits $k = 3.5$ to $k = 18$ to isolate the contributions of the different coordination shells. Due to the low signal-to-noise ratio for 0.5 wt% Pt catalysts, EXAFS experiments were carried out with 1 wt% Pt catalysts.

Hydrogen Chemisorption Measurements

Hydrogen chemisorption was carried out in a volumetric system. The sample (usually 1.5 g) was reduced for 2 h at 673 K in H_2 (when a higher reduction temperature was required, the sample was first reduced *ex situ* at the higher temperature). After reduction the sample was degassed at 673 K for 1 h in high vacuum (10^{-6} mbar). The

sample was cooled to room temperature (295 K) and the H_2 adsorption isotherm was measured by feeding decreasing amounts of H_2 (in the range 500–0 mbar) to the sample. Hydrogen chemisorption capacity was calculated by extrapolation of the hydrogen uptake to zero pressure.

The hydrogen chemisorption capacity (H/Pt ratio) was used to calculate Pt dispersions. H/Pt stoichiometry increases with decreasing particle size, because smaller particles have a higher concentration of edges and corners, where more than one hydrogen atom per metal atom can adsorb, than larger particles (18, 19). To account for this, the models described by Kip *et al*. (18) and Vaarkamp *et al*. (19) were used to calculate the fraction of metal available.

RESULTS

Stability of Different Pt Catalysts

In Fig. 1 the catalytic activities of three Pt catalysts (Pt/γ-Al_2O_3, Pt/TiO_2, and Pt/ZrO_2) are shown as a function of time on stream. The catalytic properties of these are described in earlier publications of our group (1–4) and are compiled in Table 1 (this table is discussed in detail later in this paper). Figure 1 shows that Pt/γ-Al_2O_3 and Pt/TiO_2 deactivated significantly, while Pt/ZrO_2 was stable for 50 h on stream (in this figure only the CO_2 conversion is shown; however, the CH_4 conversion and CO, H_2, and H_2O yields follow the pattern). Pt/γ-Al_2O_3 lost 95% of its initial activity during this period whereas 80% had already been lost during the first 10 h. Compared with Pt/γ-Al_2O_3, the activity of Pt/TiO_2 decreased more gradually, but also with this material the catalytic activity dropped to 25% of its original value after 50 h on stream. Pt/ZrO_2 was very stable and lost less than 1% of its activity during this period. Figure 2 illustrates the activities of 0.5 wt% Pt/ZrO_2 catalysts calcined at 925, 1025, and 1125 K as a function of time on stream. Catalytic activity and stability decreased with increasing calcination temperature. The catalyst calcined at 1125 K initially showed stable behavior (the slight increase in activity is within experimental error), which was followed, however, by significant deactivation. It is important to note here that although an increased calcination temperature had a negative influence on catalytic activity and stability, the Pt/ZrO_2 catalyst can be used at 1125 K (after low-temperature calcination) without significant deactivation.

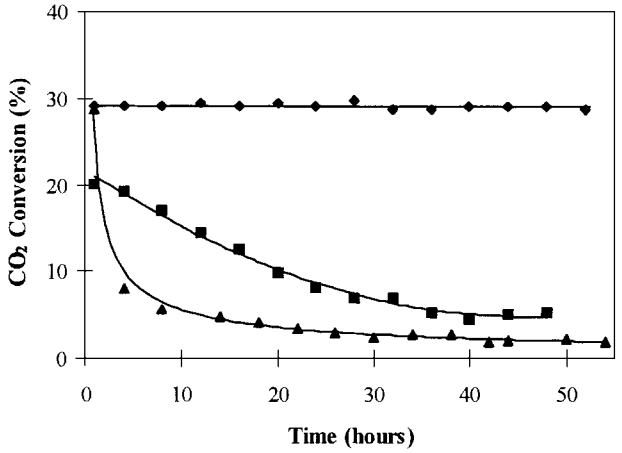

FIG. 1. Stability of different 0.5 wt% Pt catalysts at 875 K. $CO_2/CH_4/Ar/N_2 = 42/42/75/10$ ml min^{-1}, 300 mg catalyst. ◆, Pt/ZrO_2; ■, Pt/TiO_2; ▲, Pt/γ-Al_2O_3.

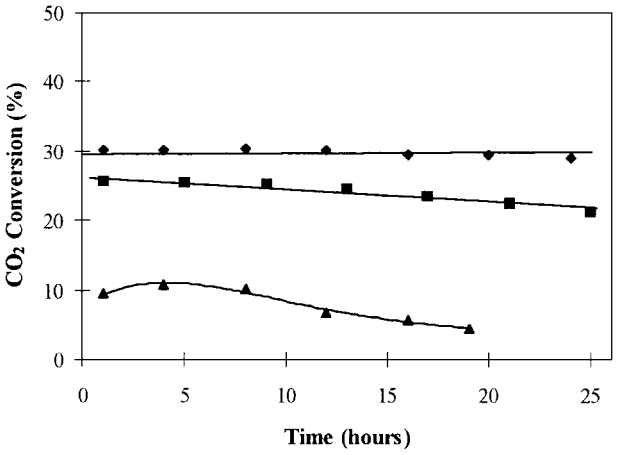

FIG. 2. Stability of 0.5 wt% Pt/ZrO_2 catalysts with different calcination temperatures. $CO_2/CH_4/Ar/N_2 = 42/42/75/10$ ml min^{-1}, 300 mg catalyst. Calcined at ◆, 925 K; ■, 1025 K; ▲, 1125 K.

Fraction of Available Pt: H_2 Chemisorption and EXAFS Measurements

In Table 1 are compiled the hydrogen chemisorption capacities of three Pt catalysts in different states [fresh, used (25 h in CO_2/CH_4 at 875 K), and regenerated (used catalyst oxidized in 5% O_2/He at 675 K and subsequently reduced at 775 K)]. The hydrogen chemisorption capacities of the used catalysts were at least an order of magnitude lower than those of the fresh catalysts. Despite the low hydrogen chemisorption capacity (H/Pt = 0.07) of the used Pt/ZrO_2, this catalyst was still active. Used Pt/γ-Al_2O_3 and Pt/TiO_2, on the other hand, showed low hydrogen chemisorption capacity (H/Pt = 0.09) and low activity. After oxidative regeneration the initial activity and hydrogen chemisorption capacity of all catalysts were restored. The process of deactivation of the fresh and reactivated Pt/γ-Al_2O_3 during 4.5 h on stream is shown in Fig. 3. The figure shows that the original activity of the catalyst is restored after oxidative treatment and also that the regenerated catalyst deactivated significantly faster than the fresh catalysts.

In Table 2 are compiled the hydrogen chemisorption capacity and average Pt–Pt coordination number for Pt/ZrO_2 calcined at different temperatures. The H_2 chemisorption capacity (and thus the fraction of Pt exposed) decreased as

TABLE 1

Some Physicochemical Properties and Activities of the Different 0.5 wt% Pt Catalysts

Catalyst	BET surface area (m^2/g)	State	Hydrogen chemisorption capacity (H/Pt)	Fraction of accessible Pt[a] (%)	CO_2 conversion (%)
Pt/ZrO_2	18	Fresh[b]	1.11	100	30
		Used[c]	0.07	7	29
		Regenerated[d]	0.90	85	30
Pt/TiO_2	7	Fresh[b]	0.25	25	20
		Used[c]	0.01	1	8
		Regenerated[d]	0.25	25	
$Pt/\gamma\text{-}Al_2O_3$	110	Fresh[b]	0.82	80	31
		Used[c]	0.09	9	3
		Regenerated[d]	0.77	75	31

[a] Calculated from H/Pt according to Kip *et al.* (18) and Vaarkamp *et al.* (19).
[b] Reduced at 775 K.
[c] After testing at 875 K for 25 h.
[d] Coke burned off in air at 675 K.

the calcination temperature increased. This was accompanied by an increase in the Pt–Pt coordination number for 1 wt% Pt/ZrO_2 (1 wt% Pt was used for EXAFS measurements due to the better signal-to-noise ratio; however, the trends for 1 and 0.5 wt% Pt are similar as shown in Table 2). The average Pt–Pt coordination number increased from 6.5 to 10.7 when the calcination temperature was raised from 925 to 1125 K.

The EXAFS results shown in Table 3 indicate that the Pt–Pt coordination numbers of fresh and used Pt/ZrO_2 and $Pt/\gamma\text{-}Al_2O_3$ catalysts were similar within experimental error. This suggests that sintering is not the major cause of the deactivation of these Pt catalysts, in agreement with the hydrogen chemisorption described above.

Carbon Formation on Pt Catalysts

To probe for the rate of carbon formation during the reforming reaction, the reaction was stopped after various times on stream (i.e., after 0.5, 1, 2, 5, 10, 25, and 50 h for $Pt/\gamma\text{-}Al_2O_3$; after 2, 5, 10, 25, and 50 h for Pt/TiO_2; and after 25 and 180 h for Pt/ZrO_2) and the amount of carbon on the catalyst was determined. Figure 4 shows the amount of carbon formed per gram of catalyst as a function of the total amount of $CO_2 + CH_4$ converted. The selectivity toward carbon increased in the order $Pt/ZrO_2 < Pt/TiO_2 < Pt/\gamma\text{-}Al_2O_3$. As also shown by us previously (1, 2), catalytic activity was proportional to the Pt–support perimeter [assuming hemispherical Pt particles (1, 2)]. Figure 5 compares the activity of Pt at the metal–support boundary with the

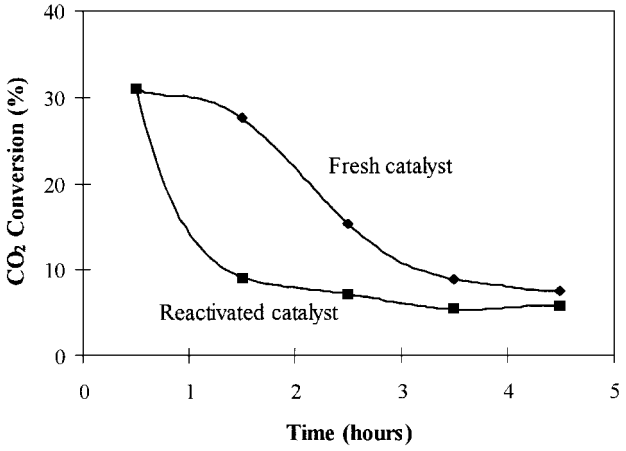

FIG. 3. Activity of 0.5 wt% $Pt/\gamma\text{-}Al_2O_3$ at 875 K. $CO_2/CH_4/Ar/N_2 = 42/42/75/10$ ml min^{-1}, 300 mg catalyst. ◆, freshly reduced catalyst; ■, reactivated by oxidation and subsequent reduction.

TABLE 2

Influence of Calcination Temperature on Pt Availability of Pt/ZrO_2

Metal loading (wt%)	Calcination temperature[a] (K)	H/Pt[b]	Fraction of accessible Pt from H/Pt[c] (%)	CN Pt–Pt[d]	Fraction of accessible Pt from CN[c,d] (%)
0.5	925	1.1	100	—	
0.5	1025	0.47	46	—	
0.5	1125	0.35	34	—	
1	925	0.89	82	6.5	86
1	1025	0.48	47	—	
1	1125	0.35	34	10.7	20

[a] All catalysts were reduced at 775 K.
[b] Measured by volumetric H_2 chemisorption.
[c] The values denote the Pt availability (%) calculated according to Kip *et al.* (18) and Vaarkamp *et al.* (19).
[d] Coordination number calculated from EXAFS.

TABLE 3

Structural Parameters from EXAFS for Fresh and Used 1 wt% Pt Catalysts

Catalyst	State	Coordination number	Fraction of accessible Pt[a] (%)	Pt–Pt distance (Å)	$\Delta\sigma^2$ ($\times 10^{-3}$ Å^2)
Pt/ZrO_2	Fresh[b]	6.5	86	2.770	1.44
	Used[c]	7	85	2.762	1.20
Pt/TiO_2	Fresh[b]	—	—	—	—
	Used[c]	10.4	26	2.761	2.00
Pt/γ-Al_2O_3	Fresh[b]	8.0	66	2.768	1.94
	Used[c]	8.5	60	2.762	1.88

[a] Calculated according to Kip *et al.* (18) and Vaarkamp *et al.* (19).
[b] Reduced at 1125 K.
[c] Used at 875 K for 25 h.

concentration of carbon formed. It can be seen from this figure that two regimes of deactivation exist with Pt/γ-Al_2O_3 and Pt/TiO_2. Initially, only slow deactivation was observed. At a certain carbon concentration, however, the catalytic activity dropped dramatically. For Pt/ZrO_2 this point of rapid deactivation was not reached even after 180 h on stream.

Table 4 shows the amount of carbon formed on the different catalysts after 25 h of reaction. For comparison, the amounts of carbon formed on the blank supports, under reaction conditions, are also included in the table. It is seen that carbon was formed on the blank supports and on the Pt-containing catalysts. The rate of coking decreased in the order Pt/γ-$Al_2O_3 > Pt/TiO_2 > Pt/ZrO_2$, which coincides with the order of increasing stability. In the same table are compiled the fractions of the surface area of the catalysts that were covered by carbon at the point of rapid deactivation

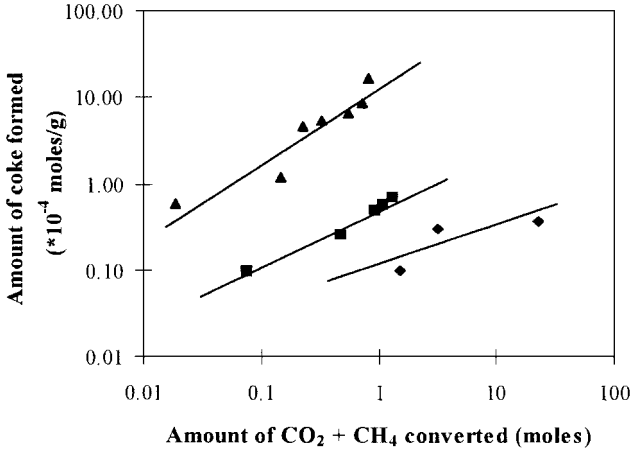

FIG. 4. Amounts of coke formed per gram of catalyst as a function of the total amount of $CO_2 + CH_4$ converted on different 0.5 wt% Pt catalysts at 875 K. ◆, Pt/ZrO_2; ■, Pt/TiO_2; ▲, Pt/γ-Al_2O_3.

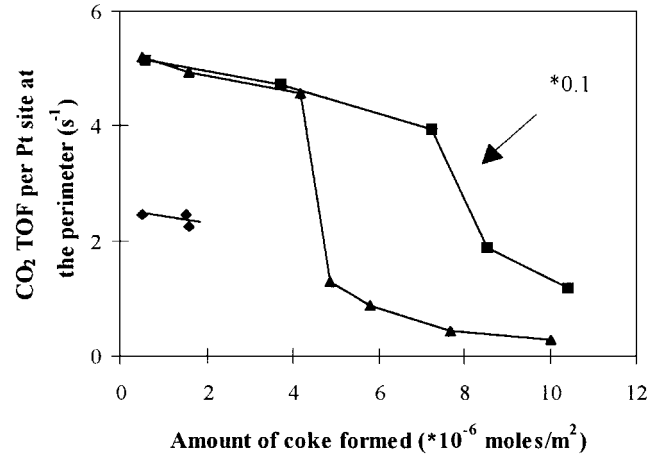

FIG. 5. Catalytic activity of different Pt catalysts as a function of the amount of carbon deposited on the catalyst at 875 K. ◆, Pt/ZrO_2; ■, Pt/TiO_2; ▲, Pt/γ-Al_2O_3.

and after 25 h on stream (see Fig. 5). It can be seen that even in the case of severe deactivated catalysts (Pt/γ-Al_2O_3 and Pt/TiO_2) only a small fraction of surface area (a maximum 28%) was covered with carbon.

In Table 5 are listed the amounts of carbon formed on 0.5 wt% Pt/ZrO_2 catalysts calcined at different temperatures (different Pt particle sizes). It can be seen that the amounts of carbon formed on the differently calcined catalysts were similar, when the calcination temperature was raised from 925 to 1125 K. However, the selectivity to carbon (i.e., moles of carbon formed/moles of feed converted) increased significantly.

DISCUSSION

Hydrogen Chemisorption

The hydrogen chemisorption capacity of Pt/ZrO_2, and hence the fraction of exposed Pt in different Pt catalysts

TABLE 4

Coke Deposition at 875 K on Different Catalysts and Supports

Catalyst	Coke from CO_2/CH_4 after 25 h[a] ($\times 10^{-4}$ mol/g)	Fraction of catalyst surface covered with coke after 25 h	Fraction of catalyst surface covered with coke at point of rapid deactivation
Pt/ZrO_2	0.3	0.005	—
ZrO_2	0.8	0.01	—
Pt/TiO_2	0.5	0.25	0.20
TiO_2	1.3	0.65	—
Pt/γ-Al_2O_3	8.9	0.28	0.14
γ-Al_2O_3	2.1	0.07	—

[a] On the bare supports no conversion or product formation was observed by means of GC analysis.

TABLE 5

Coke Deposition at 875 K on 0.5 wt% Pt/ZrO_2 Calcined at Different Temperatures

Catalyst	Coke from CO_2/CH_4 after 25 h ($\times 10^{-4}$ mol/g)	Coke selectivity[a] ($\times 10^{-6}$ mol/mol)
925	0.31	9.4
1025	0.41	16
1125	0.43	28

[a] Coke selectivity = moles of coke formed per gram catalyst/moles of $CO_2 + CH_4$ converted.

(compiled in Table 2), decreased with increasing calcination temperature. This was also observed when the fraction of metal exposed was estimated from the average particle size calculated from EXAFS. Thus, we conclude that the increasing calcination temperature caused sintering of the Pt particles. The decrease in Pt availability was accompanied by a lowering of the initial activity (see Fig. 2).

The hydrogen chemisorption capacities of catalysts after different stages of reaction are compiled in Table 1. After 25 h of reaction the hydrogen chemisorption capacities of all catalysts were very low compared with those of the fresh catalysts. For Pt/TiO_2 and Pt/γ-Al_2O_3 (but not for Pt/ZrO_2) this was accompanied by a decrease in activity (see also Figs. 1 and 2). Because the hydrogen chemisorption capacity of the catalysts and their activity were restored after a mild oxidative treatment (5% O_2/He at 675 K) we conclude that sintering did not occur. Moreover, the Pt–Pt coordination numbers of used catalysts (without oxidative treatment) calculated from EXAFS did not differ from those of the freshly reduced samples (Table 3). Thus, it was concluded that the low hydrogen chemisorption capacity of the catalysts after 25 h of reaction was caused by blocking of the metal by carbon deposits. Because Pt/ZrO_2 did not deactivate, even though Pt was covered with carbon (Tables 1 and 3), we conclude that at least part of the carbon on this catalyst must be reactive. In contrast, Pt/γ-Al_2O_3 and Pt/TiO_2 lost nearly all activity, indicating a much lower concentration of reactive carbon or a lower overall reactivity of the carbon.

Carbon Formation on Pt Catalysts

The results discussed thus far indicate that carbon deposition and not sintering causes the reduced hydrogen chemisorption capacity of the used catalysts. However, the overall amount of carbon varied drastically (see Table 4) despite the similarly low fractions of metal atoms exposed in the used samples. This is a result of carbon being formed on the pure support and on the metal-containing catalysts (Table 4).

The relation between the amount of carbon formed on the pure support and on the catalysts is complex. The amounts of carbon deposited on the oxides increased in the sequence $ZrO_2 < TiO_2 < Al_2O_3$. For Pt/ZrO_2 and Pt/TiO_2 the amount of carbon formed on the catalysts is lower than that on the support alone, while for Pt/γ-Al_2O_3 it is higher. We attribute this to the combination of Lewis acid sites and metal particles. For the former two catalysts, Pt seems to selectively block Lewis acid sites [as suggested earlier by Masai *et al.* (20)], while for Pt/γ-Al_2O_3 a significant fraction remains after Pt deposition as seen from a comparison of IR spectra of sorbed pyridine on Pt/γ-Al_2O_3 and Pt/ZrO_2. The presence of Lewis acid sites facilitates the cleavage of methane C–H bonds (21–25). Then, hydrogen desorbs through proton–hydride recombination, carbon remaining on the surface. The synergistic action of Pt and the γ-Al_2O_3 support with respect to carbon formation seems to relate to easier hydrogen desorption, as, e.g., observed with zeolite-catalyzed dehydrocyclization reactions (21, 22). In the absence of Pt, coking on the support is limited by the desorption of the hydrogen formed. When Pt is added, hydrogen desorption is enhanced via recombination on Pt.

The stability of the carbon toward oxidation aids in the estimation of the fraction of carbon on the metal and on the support. In an elegant study Barbier *et al.* identified two types of "carbon" in cyclopentane reforming over Pt/γ-Al_2O_3 via their stability toward oxidation (23, 26). The carbon located on the metal could be removed in oxygen at 575 K, whereas the carbon formed on the support was less reactive toward oxygen and could be removed only at 725 K. Figure 6 shows the results of oxygen pulsing at two subsequent temperatures over used Pt/γ-Al_2O_3. At low temperature (675 K) only 10% of the carbon on Pt/γ-Al_2O_3 could be removed, while the remaining 90% was removed at high temperature (1125 K). This indicates that a large fraction of the carbon is located on the support. Because the samples were degassed in He at 1125 K prior to O_2 pulsing and IR spectroscopic studies revealed that carbonates

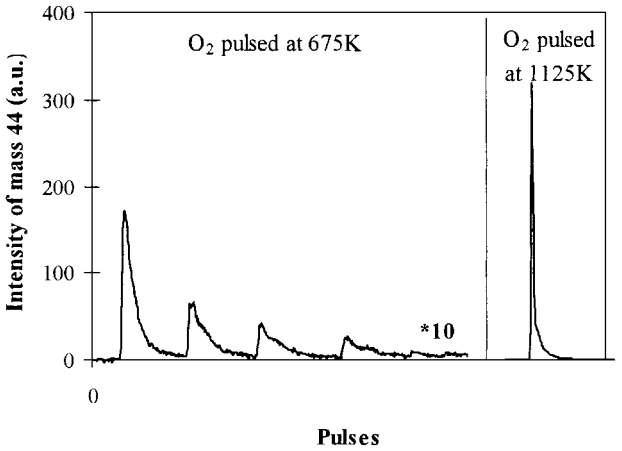

FIG. 6. Coke oxidation on Pt/γ-Al_2O_3 (50 mg) used for 5 h. $CO_2/CH_4/Ar/N_2 = 42/42/75/10$ ml min^{-1}.

decomposed rapidly above 600 K in He, it is concluded that the carbon does not exist in the form of a carbonate.

In most of the cases hydrocarbon activation on oxidic materials is strictly related to the nature, concentration, and strength of the acid sites (21–24). In the case of methane all (partly) dehydrogenated intermediates (CH_x) will contribute to carbon formation unless they can be desorbed as radicals, as discussed vividly for the case of oxidative methane coupling (27–30). This latter route may not be very pronounced on our present catalysts. Consequently, this suggests that some acid sites must exist on the support. Indeed, IR spectroscopy of adsorbed pyridine revealed a higher concentration of Lewis acidic sites on Pt/γ-Al_2O_3 compared with ZrO_2. Thus, we conclude that the higher concentration of acid sites on the support increased the amount of carbon formed. It is calculated (Table 4) that at the point of rapid deactivation (Fig. 5) for Pt/γ-Al_2O_3, only 14% of the support is covered with carbon. Therefore, it is unlikely that carbon formed on the support is the sole route to catalyst deactivation. If the support does not selectively coke around the metal particles then these results indicate that carbon originating from the metal is overgrowing the Pt–support perimeter and is the predominant factor in catalyst deactivation.

It has been suggested that the ability to activate CO_2 (as carbonate) on the support is essential for high activity (1, 2). Auroux and Gervasini showed that the heat of CO_2 adsorption varies with the support (31). On ZrO_2 two types of strongly bound CO_2 were observed (with heats of adsorption of 60 and 125 kJ/mol). For γ-Al_2O_3 a lower heat of adsorption (30 kJ/mol) was found. The heat of adsorption on TiO_2 is similar although somewhat lower than on ZrO_2. We therefore speculate that the lower stability of the carbonates formed on Al_2O_3 and TiO_2 compared with those on ZrO_2 results in fewer or less reactive forms of carbonates (i.e., on Al_2O_3 and TiO_2 the desorption rate is too high; therefore, the concentration of carbonates is relatively low). This, in turn, lowers the rate of carbon removal without influencing the rate of carbon formation (mainly determined by the pure metal), eventually causing an overgrowth of the catalytically active metal perimeter by carbon from the side of the metal that quenches the activity.

The two regions of deactivation observed on Pt/γ-Al_2O_3 and Pt/TiO_2 (see Fig. 5) indicate that at least two reaction routes of deactivation exist. The carbon deposited in the initial stage has a weak negative influence on catalytic activity. This initial phase of slow deactivation is attributed to a singular blocking of active metal sites with unreactive carbon or oxidic sites for CO_2 activation at the metal–support boundary. The rapid deactivation is then explained by overgrowth of the metal perimeter with carbon of low activity. Such less reactive carbon may be formed from more reactive carbon as, e.g., shown for CO methanation on Ni (32).

The carbon located on the support and not removed during mild reactivation (see Fig. 6 and Discussion) allows us to explain the faster deactivation of regenerated Pt/γ-Al_2O_3. Because low-temperature oxidation restored the activity of the catalyst (Fig. 3) and its hydrogen chemisorption capacity, it appears that the metal particle and the perimeter are accessible for reaction after regeneration. If only the carbon formed around the metal particle is removed during the mild reactivation, it is likely that progressive coking on the support in combination with carbon formed on the metal blocks this reactivated zone rapidly. This implies that the carbon on the oxide surface (not regenerated during the mild treatment) participates in carbon formation. This is supported by observations in the literature (33). Reactivation of Pt/γ-Al_2O_3 at 875 K to remove more carbon from the support led to significantly lower catalyst activity. This is due to sintering of Pt during oxidative treatment probably because the local temperatures exceeded 875 K because of the exothermicity of the reaction. Note that increasing the calcination temperature of a Pt/γ-Al_2O_3 increased Pt particle size (see H_2 chemisorption and EXAFS measurements).

We have previously shown that the catalytic activity of Pt/ZrO_2 is directly proportional to the perimeter of the Pt particles (1, 2). The decrease in catalytic activity induced by varying the calcination temperature is fully compatible with that interpretation. Larger particles have a higher total surface area-to-perimeter ratio than smaller particles. This has only a minor influence on the carbon produced on the support, but leads to more carbon formed on the metal which finds a smaller fraction of surface metal atoms where it can be oxidized to CO (i.e., the perimeter). As a consequence more carbon accumulates at the metal [and eventually is transformed to an unreactive form (32, 34)] which, finally, also blocks the active perimeter zone.

CONCLUSIONS

The stability of Pt catalysts for dry CO_2/CH_4 reforming depends crucially on the support. The stability of the catalysts increased in the order Pt/γ-$Al_2O_3 \ll$ Pt/TiO_2 < Pt/ZrO_2. Pt/ZrO_2 is a stable catalyst and operates with only minor deactivation. For the Pt-based catalysts the site of catalytic activity had been previously identified to be the zone at the metal–support interface (1, 2). The major cause of deactivation of these Pt catalysts is blocking of active sites by carbon deposited from methane. Carbon is formed on the support and on the metal. The rates of carbon formation and deactivation of the catalysts depend on the stability of the carbonates formed from CO_2 (which will react with the carbon species formed form methane) on the support. Decreasing the stability of the carbonate (e.g., by exchanging ZrO_2 for γ-Al_2O_3) may contribute to increasing the rate of overgrowth of the Pt–support perimeter by carbon

formed on the metal. With increasing Pt particle size, the rates of carbon formation (on the metal) and removal (on the perimeter) shift in favor of carbon formation (note that also the texture of the particles might change with changing particle size; this can also increase the rate of carbon formation). This causes an additional source of deactivation through pronounced carbon accumulation on the metal and transformation of this carbon into a nonreactive form. Thus, on catalysts with larger Pt particles the balance between the formation of carbon and its oxidation via surface carbonate is perturbed. The results show that by fine-tuning the particle size of the metal and the acid–base properties (providing enough strength to stabilize carbonate formation and low enough concentration of acid sites to avoid pronounced methane decomposition), Pt-based supported catalysts can be prepared that are highly stable during methane reforming with carbon dioxide.

ACKNOWLEDGMENTS

This project was supported by the European Union, Joule II Programme, Subprogramme "Energy from Fossil Sources: Hydrocarbons," Contract JOU2-CT92-0073. The EXAFS measurements were carried out at the SRS, Daresbury Laboratory, United Kingdom, through Grant 27/251. This work was performed under the auspices of NIOK, The Netherlands Institute for Catalysis (Report UT-98-1-02).

REFERENCES

1. Bitter, J. H., Seshan, K., and Lercher, J. A., *J. Catal.* **171**, 279 (1997).
2. Bitter, J. H., Seshan, K., and Lercher, J. A., *J. Catal.* **176**, 93 (1998).
3. Bitter, J. H., Seshan, K., van Ommen, J. G., and Lercher, J. A., *Catal. Today* **29**, 349 (1996).
4. Lercher, J. A., Bitter, J. H., Hally, W., Niessen, W., and Seshan, K., *Stud. Surf. Sci. Catal.* **101**, 463 (1996).
5. Bradford, M. J. C., and Vannice, M. A., *Appl. Catal. A* **142**, 97 (1996).
6. Zhang, Z., Verykios, X. E., MacDonald, S. M., and Affrossman, S., *J. Phys. Chem*. **100**, 744 (1996).
7. Udengaard, N. R., Bak Hansen, J.-H., Hanson, D. C., and Stal, J. A., *Oil Gas J.* **90**, 62 (1992).
8. Rostrup-Nielsen, J. R., and Bak Hansen, J.-H., *J. Catal.* **144**, 38 (1993).
9. Stagg, S. M., Salazar, E. R., Padro, C., and Resasco, D. E., *J. Catal.* (1997).
10. Richardson, J. T., and Paripatyadar, S. A., *Appl. Catal.* **61**, 293 (1990).
11. Tsipouriari, V. A., Estathiou, A. M., Zhang, Z. L., and Verykios, X. E., *Catal. Today* **21**, 579 (1994).
12. Seshan, K., ten Barge, H. W., Hally, W., van Keulen, A. N. J., and Ross, J. R. H., *Stud. Surf. Sci. Catal.* **81**, 285 (1994).
13. Ashcroft, S. T., Cheetham, A. K., Green, M. L. H., and Vernon, P. D. F., *Nature* **352**, 225 (1991).
14. Swaan, H. M., Kroll, V. C. H., Martin, G. A., and Mirodatos, C., *Catal. Today* **21**, 571 (1994).
15. Teuner, S., *Hydroc. Proc.* **64**, 106 (1985).
16. Kurz, G., and Teuner, S., *Erdol. Kohle* **43**(5), 171 (1990).
17. (a) Van Keulen, A. N. J., Seshan, K., Hoebink, J. H. B. J., and Ross, J. R. H., *J. Catal.* **166**, 306 (1997). (b) Van Keulen, A. N. J., Ph.D. thesis, University of Twente, 1996.
18. Kip, B. J., Duivenvoorden, F. B. M., Koningsberger, D. C., and Prins, R., *J. Catal.* **105**, 26 (1987).
19. Vaarkamp, M., Grondelle, J. V., Miller, J. T., Sajkowski, D. J., Modica, F. A., Lane G. S., Gates, B. C., and Koningsberger, D. C., *Catal. Lett.* **6**, 369 (1990).
20. Masai, M., Kado, H., Miyake, A., Nishiyama, S., and Tsuruya, S., *in* "Methane Conversion" (D. M. Bibby, D. Chang, R. F. Howe, and S. Yurchak, Eds.), Elsevier Science, Amsterdam, 1988.
21. Iglesia, E., Baumgartner, J. E., and Price, G. L., *J. Catal.* **134**, 549 (1992).
22. Iglesia, E., and Baumgartner, J. E., *Catal. Lett.* **21**, 55 (1993).
23. Barbier, J., *Appl. Catal.* **23**, 225 (1986).
24. Narbeshuber, T. F., Brait, A., Seshan, K., and Lercher, J. A., *Appl. Catal.* **146**, 119 (1996).
25. Narbeshuber, T., Ph.D. thesis, University of Twente, 1995.
26. Barbier, J., Corro, G., and Zhang, Y., *Appl. Catal.* **13**, 245 (1985).
27. McCarthy, J. G., McEwen, A. B., and Quinlan, M. A., *in* "New Developments in Selective Oxidation" (G. Centi and F. Trifiro, Eds.), *Stud. Surf. Sci. Catal.* **55**, 405 (1990).
28. Zanthoff, H., and Baerns, M., *Prepr. Am. Chem. Soc. Div. Pet. Chem.* **37**, 167 (1992).
29. Shi, C., Hatano, M., and Lunsford, J. H., *Catal. Today* **13**, 353 (1992).
30. Reyes, S. C., Iglesia, E., and Kelkar, C. P., *Chem. Eng. Sci.* **48**, 2643 (1993).
31. Auroux, A., and Gervasini, A., *J. Phys. Chem*. **97**, 6371 (1990).
32. Goodman, D. W., *J. Vac. Sci. Technol.* **20**(3), 522 (1982).
33. Hirschon, A. S., Wu, H.-J., Wilson, R. B., and Malhotra, R., *J. Phys. Chem*. **99**, 17483 (1995).
34. Van Langeveld, A. D., Van Delft, F. C. M. J. M., and Ponec, V., *Surf. Sci.* **135**, 93 (1983).